Spindle position dictates division site during asymmetric cell division in moss

Elena Kozgunova[1]*, Mari W. Yoshida[1] and Gohta Goshima[1,2]*

[1]Division of Biological Science, Graduate School of Science, Nagoya University, Furo-cho, Chikusa-ku, Nagoya, Aichi 464-8602, Japan

[2]Sugashima Marine Biological Laboratory, Graduate School of Science, Nagoya University, Sugashima, 429-63, Toba 517-0004, Japan

*Correspondence should be addressed to kozgunova@gmail.com; goshima@bio.nagoya-u.ac.jp

Phone & Fax: +81 52-788-6174

Abstract

Asymmetric cell division (ACD) underlies the development of multicellular organisms. The division site in plant cells is predetermined prior to mitosis and the localization of the mitotic spindle is considered static, unlike in animal ACD, where the cell division site is defined by active spindle-positioning mechanisms. Here, we isolated a novel mutant of the microtubule-associated protein TPX2 in the moss *Physcomitrella patens* and observed abnormal spindle motility, which led to inverted asymmetric division during organ development. This phenotype was rescued by restoring endogenous TPX2 function and, unexpectedly, by depolymerizing actin filaments. Thus, we identify an active spindle-positioning mechanism involving microtubules and actin filaments that sets the division site in plants, which is reminiscent of the acentrosomal ACD in animals, and suggests the existence of a common ancestral mechanism.

Introduction

Chromosome segregation during mitosis and meiosis is driven by the complex microtubule (MT)-based apparatus known as the spindle. Animal spindles are known to be mobile and their final position corresponds to the future cytokinesis site, which in turn, could determine daughter cell fate after asymmetric division. The mechanism whereby the spindle is positioned and spatially controls the assembly of the cytokinetic machinery is well studied in animals and the critical roles of force-generating machineries, such as dynamic MTs, actin, and motor proteins, have been elucidated (Bergstralh et al., 2017; Kiyomitsu, 2019). However, in plants, it was long believed that the pre-prophase band (PPB), a plant-specific MT-actin belt formed prior to mitotic entry, determines the future cell division site (Buschmann and Müller, 2019; Rasmussen and Bellinger, 2018; Verma, 2001). The mitotic spindle always forms perpendicular to and at the site of the PPB, perhaps by the action of bridging MTs that connect the spindle to the former PPB site (Ambrose and Cyr, 2008). The spindle position is considered to be static, unless a strong

force (1600-3350 × *g*) is applied through centrifugation, which also causes other cytoplasmic components to translocate (Arima et al., 2018; Ôta, 1961). The static nature of spindles is consistent with the fact that plants lack centrosomes, which play key roles in spindle translocation in animal somatic cells (Bergstralh et al., 2017; Kiyomitsu, 2019). Multiple proteins co-localized to the PPB are required to establish and maintain the cortical division zone (CDZ), towards which the cytoskeleton-based cytokinetic machinery, known as the phragmoplast, expands while recruiting cell plate components (Müller, 2019; Smertenko et al., 2017).

However, the essential role of the PPB in determining the cell division site has recently been challenged. *Arabidopsis thaliana* mutants lacking the PPB do not show severe defects in oriented cell division, as anticipated from the prevailing model described above (Schaefer et al., 2017). Although spindle orientation is more variable in the PPB-null mutants, the mean value is similar to the mean value of wild-type plants. Consequently, global tissue organization and plant morphogenesis are normal in the absence of the PPB.

The moss *Physcomitrella patens* is an attractive model plant in studying PPB-independent division plane determination, as most cell types naturally lack PPBs, but are capable of oriented cell division and patterning into complex 3D structures, such as gametophores (leafy shoots) (Kosetsu et al., 2017; Moody et al., 2018). We have previously shown that the MT structure, called the gametosome, appears in the cytoplasm transiently at prophase and acts as the determinant of spindle orientation (Kosetsu et al., 2017). However, gametosomes are dispensable for spindle MT generation or spindle positioning.

In animal cells, the mitotic spindle is assembled through rapid MT nucleation and amplification aided by multiple proteins, including γ-tubulin, augmin and TPX2 (targeting factor for Xklp2) (Petry, 2016). Previous study in *A. thaliana*, using a combination of knockout and cross-species antibody injection, suggested TPX2 to be an essential gene (Vos et al., 2008). However, these results were recently questioned when several viable AtTPX2 t-DNA insertion mutants were obtained (Boruc et al., 2019). Beside canonical TPX2, several TPX2-like genes, lacking one or more functional domains, were identified in *A. thaliana*. Among them, TPX2L3 lacks C-terminal kinesin-biding motif but is strongly associated with Aurora kinases and essential for embryogenesis (Boruc et al., 2019). However, how TPX2 contributes to spindle formation and MT amplification in plant cells remains unknown. In this study, we aimed to characterize TPX2 function in the spindle assembly in *P. patens*, wherein many research tools, including inducible RNAi, endogenous gene tagging and highly efficient CRISPR are easily applicable (Leong et al., 2018; Yamada et al., 2016; Yi and Goshima, 2019). In addition to TPX2's role in the MT amplification during early mitosis, we found an unexpected function of TPX2 in maintaining spindle position during asymmetric cell division in gametophores.

Results & Discussion

We identified five genes homologous to *TPX2* in the *P. patens* genome using a BLAST search and named them *TPX2-1* to *-5* (Figure 1A). TPX2-1 to -4 proteins show high similarity to canonical TPX2 in seed plants (e.g., *A. thaliana, Orysa sativa*), whereas TPX2-5 appears to have lost the N-terminal Aurora-binding motif (Boruc et al., 2019; Tomaštíková et al., 2015; Vos et al., 2008), but retains the highly conserved C-terminal domains and to certain extent, γ-tubulin activation motifs (Alfaro-Aco et al., 2017) (Figure 1A, B). During mitosis, endogenous TPX2-1, -2, and -4 proteins fused with fluorescently tagged Citrine ("Cit") or mNeonGreen ("NG") in-frame at the C- or N-terminal, were enriched at the polar region of the spindle and phragmoplast, suggesting that they preferentially bind to MT minus ends (Figure 1C, Supplemental Figure 1, Supplemental Video 1). A similar localization has been reported for *Arabidopsis* TPX2 (Boruc et al., 2019; Vos et al., 2008). TPX2-5 was observed as dim speckles in the spindle and showed more uniform binding to phragmoplast MTs (Figure 1C, Supplemental Figure 1E, Supplemental Video 1). Unlike TPX2 of animals or seed plants (Boruc et al., 2019; Vos et al., 2008), none of the TPX2 proteins of *P. patens* were sequestered in the nucleus during interphase (Supplemental Figure 2A, B).

The similarity in amino acid sequences and intracellular localization suggested that TPX2-1 to -4 have redundant functions. We, therefore, simultaneously targeted these genes using a previously established CRISPR/Cas9 protocol (Leong et al., 2018). We isolated a line, named *TPX2 1-4Δ*, in which frameshifts were introduced to all four *TPX2* genes in the exons present in all transcript variants identified in the Phytozome database (Supplemental Figure 3A). The *TPX2 1-4Δ* line developed protonema (tissue comprised of frequently dividing tip-growing cells) and gametophores in a similar manner to the parental "GH" line (control, Supplemental Figure 3B). We then attempted to knock out the *TPX2-5* gene in the *TPX2 1-4Δ* background, by means of homologous recombination. However, we could not isolate a knockout line after multiple attempts. Given the high efficiency of homologous recombination in *P. patens*, the *TPX2-5* gene is likely essential in the *TPX2 1-4Δ* background.

Nonetheless, in our attempt to knockout the *TPX2-5* gene, we isolated a line with dwarf gametophores and defective leaf development (Figure 2A, Supplemental Figures 3B, 4E). In this line, the original *TPX2-5* gene was replaced with a hygromycin cassette, as confirmed by PCR and sequencing (Supplemental Figure 3C, D). However, DNA was amplified by PCR using *TPX2-5*'s "internal" primers, and we confirmed that all exons from *TPX2-5* gene remained in the genome by sequencing. These data suggested that the *TPX2-5* gene removed from the original locus was re-inserted in the genome, possibly through micro-homology recombination, resulting in compromised expression of the TPX2-5 protein. Hereafter, this hypomorphic line is referred to as "*TPX2-5 HM*".

To test if the line indeed represents a hypomorphic mutant of *TPX2*, we performed a rescue experiment in which a frameshift repair construct targeting *TPX2-4* was transformed into the *TPX2-5 HM* line (Supplemental Figure 4A). The selected lines in

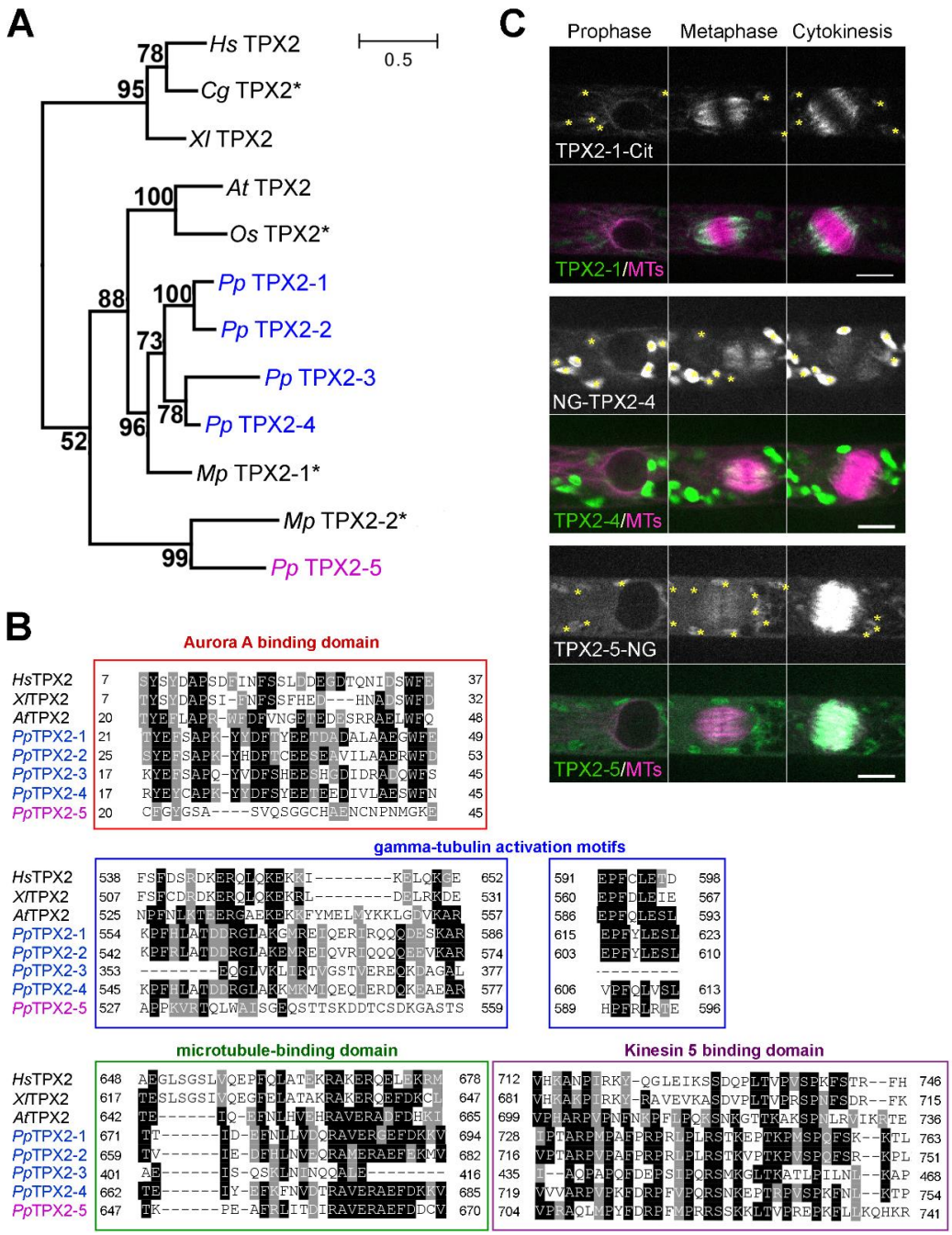

Figure 1. TPX2 homologues and their localization in *P. patens*

(A) Phylogeny analysis revealed two distinct groups of TPX2 proteins in *P. patens*: Pp *TPX2-1* to *-4* (blue), which are more similar to *TPX2* genes from seed plants, and atypical *TPX2-5* (magenta). Asterisks mark predicted proteins, numbers show bootstrap values. Bar, 0.5 amino acid substitutions per site. Note that AtTPX2L3 and AtTPX2L2 could not be added to this tree, since they lack the C-terminal region that is conserved in canonical TPX2 proteins. Hs: *Homo sapiens*, Gg: *Gallus gallus*, Xl: *Xenopus laevis*, At: *Arabidopsis thaliana*, Os: *Oryza sativa*, Pp: *Physcomitrella patens*, Mp: *Marchantia polymorpha*. **(B)** Alignment of TPX2 proteins. Conserved residues are boxed, whereas similar amino acids are hatched. **(C)** Localization of endogenous TPX2-1-Citrine, mNeonGreen-TPX2-4 and TPX2-5-mNeonGreen. More uniform spindle localization was detected for TPX2-5. Asterisks indicate autofluorescent chloroplasts. Bar, 10 µm. The full version of mitotic localization data is presented in Supplemental Figure 1.

which construct integration was confirmed by PCR no longer showed a mitotic delay or dwarf gametophore phenotype (Supplemental Figure 4B-E). These results strongly suggested that the observed abnormal phenotypes were indeed due to TPX2 malfunction.

We next aimed to determine if TPX2 plays a role in the mitosis of gametophore cells, as dwarf gametophores are the most prominent phenotype of the *TPX2-5 HM* line (Figure 2A). Dwarf organ development in plants is often associated with defective cytokinesis (Martinez et al., 2017). Thus, we first used the lipophilic dye, FM4-64, to visualize cell plates in gametophore initials (stem cells) after the first cell division. We observed that the orientation and position of the cell plate shifted to the basal side of the gametophore initial in 11 out of 19 cells in the *TPX2-5 HM* mutant, dramatically skewing the ratio between apical and basal daughter cells. Importantly, this was due to defective TPX2, as the cell plate positioning was normal in the aforementioned repair lines (Figure 2B, C).

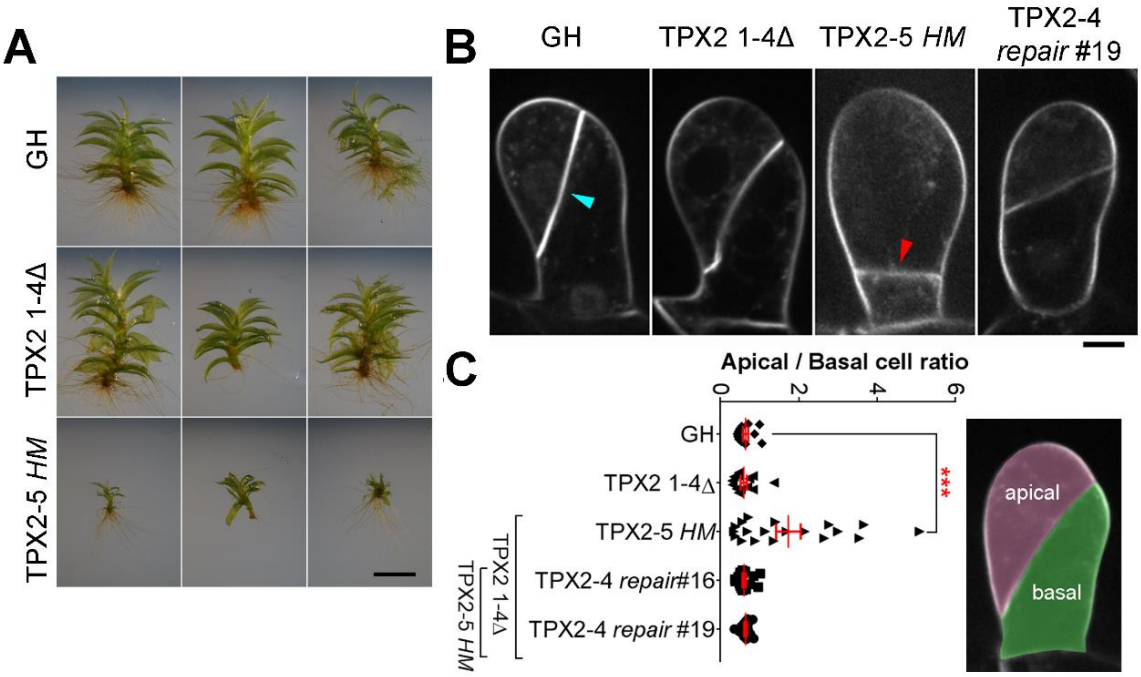

Figure 2. Abnormal cell division site in the gametophore initial of a TPX2 mutant
(A) Representative photos of gametophores after 4 weeks of culture of GH (control), *TPX2 1-4Δ*, and *TPX2-5 HM* lines. Bar, 2 mm. **(B)** Gametophore initial at the 2-cell stage stained with FM4-64 dye. Normal and defective cell plate positions are indicated with cyan and red arrowheads, respectively. Bar, 10 µm **(C)** The apical/basal cell ratio was estimated as the apical cell area (pink) divided by the basal cell area (green), measured during the 2-cell stage (n = 12, 13, 19, 18, and 14 for GH, *TPX2 1-4Δ*, *TPX2-5 HM*, *TPX2-4 repair* #16, and *TPX2-4 repair* #19 lines, respectively, ***p = 0.0004 one-way Anova with Dunnetts multiple comparison test). Error bars indicate SEM.

To observe mitotic MTs in gametophore initial cells, we introduced another marker, mCherry-tubulin, to *TPX2-5 HM*, *TPX2 1-4Δ*, and control GH lines (note that histone and tubulin were labelled with the same color). The majority of gametophore initial cells in the *TPX2-5 HM* line formed a bipolar spindle (90%; n = 19; Figure 3A, B), although slightly smaller than the spindle in the control or *TPX2 1-4Δ* lines (Figure 3C). Strikingly, we observed that the bipolar metaphase spindle moved unidirectionally over 5 µm to the basal side in 73% of *TPX2-5 HM* cells (Figure 3A, D, Supplemental Video 2). Consequently, the phragmoplast formed close to the basal edge. We concluded that defective spindle positioning after NEBD was the major cause for the abnormal cell plate position in the gametophore initials of the *TPX2-5 HM* line.

In animals, spindle motility relies on MTs and/or actin. To test the involvement of the cytoskeleton in spindle motility, we first partially depolymerized MTs in the *TPX2-5 HM* line using low-dosage oryzalin (200 nM), a MT-destabilizing drug. Upon treatment, the spindle behaviors were more variable and showed overall differences from untreated cells. Most notably, in 5 of 16 cells, we observed that the spindle had shifted towards the apical side of the cells, which was never observed in untreated cells (Figure 3D). Additionally, the average basal spindle motility decreased. In the presence of oryzalin, 6 out of 16 spindles moved slower than 1 µm/min, whereas only 1 out of 15 did so in untreated cells. These data suggested that MTs contribute to spindle motility to a certain extent.

We next investigated the effect of F-actin disruption on spindle motility by adding latrunculin A, an actin inhibitor. Previously, it was shown that actin inhibition does not affect spindle morphology, orientation, or positioning in the control line (Kosetsu et al., 2017). However, latrunculin A treatment completely (20 out of 20 cells) suppressed the basal motility of the spindle in the *TPX2-5 HM* mutant line (Figure 3D, Supplemental Video 2). These results suggested an interplay between MTs and actin filaments in spindle positioning.

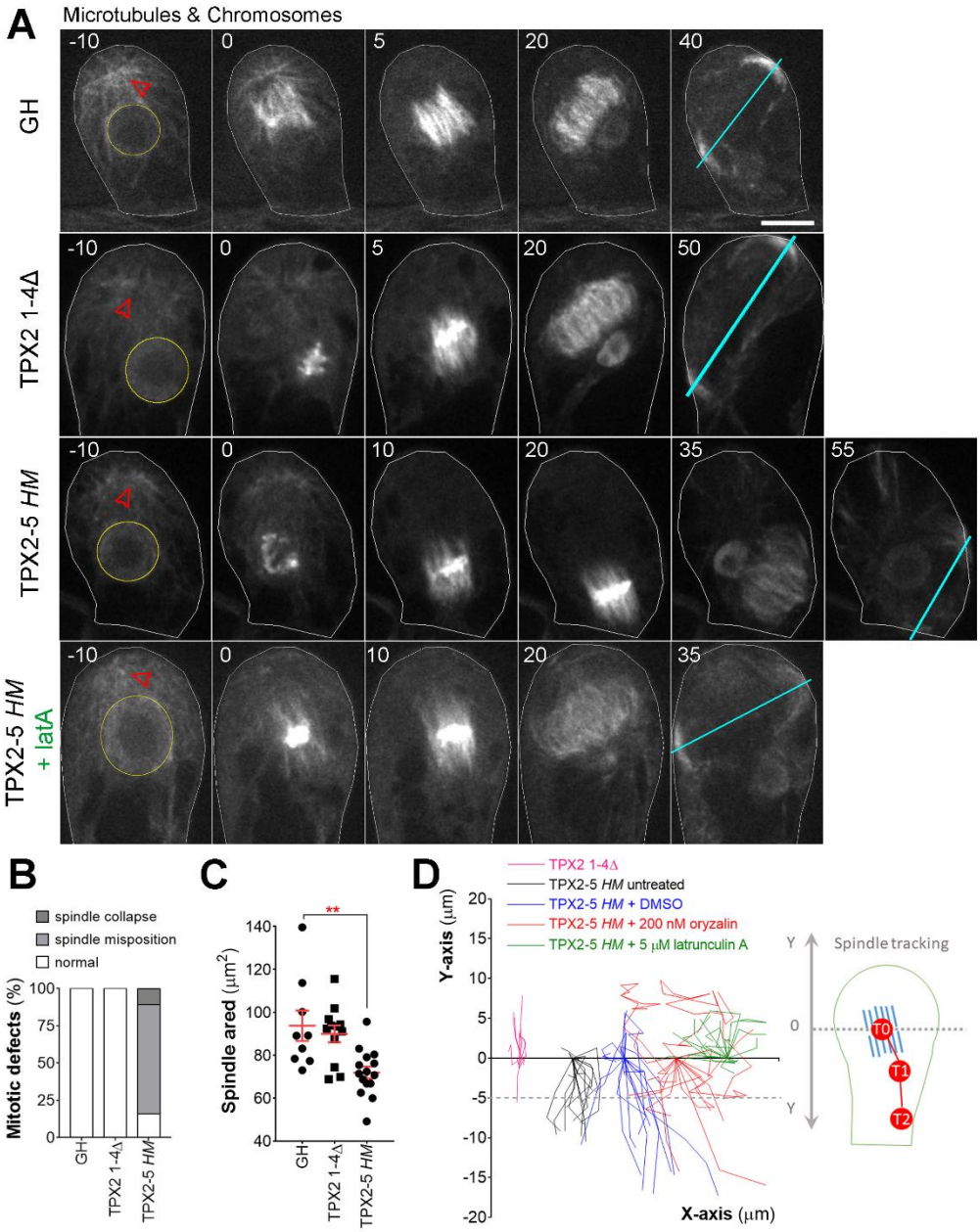

Figure 3. Spindle position was actively maintained through the interplay between microtubules and F-actin

(A) Live-cell imaging of the first asymmetric division in the gametophore initial revealed a link between the metaphase spindle and phragmoplast positioning. The positions of the nucleus and gametosome (prophase MTOC appeared in the apical cytoplasm) are indicated with yellow circles and red arrowheads, respectively. Cyan lines show the position and orientation of the phragmoplast. Cell borders are outlined with white lines. Bar, 10 μm. **(B)** The frequency and type of spindle defects in gametophore initial mitosis observed in GH (control), *TPX2 1-4Δ*, and *TPX2-5 HM* lines. **(C)** Area occupied by the metaphase spindle (spindle size) in gametophore initials. (mean ± SEM; ***p* = 0.0029, two-tailed Student's t-test) **(D)** Tracking of the spindle center position from NEBD to anaphase onset. We assigned the starting position as Y = 0 and different X positions for each sample group. Note that after 5 μM latrunculin A treatment, spindles never showed motility towards the basal end of the cell, i.e. negative Y-values. Each line represents spindle movement in a single cell. More than 12 cells were observed for each sample group in three or more independent experiments.

To gain insights into the molecular function of moss TPX2 towards MTs, we aimed to perform a detailed analysis of cell division phenotypes in the mutant with the greatest effect. To this end, we selected an inducible *TPX2-5* RNAi line in the *TPX2 1-4Δ* background. Since RNAi induction almost completely inhibited cell growth and gametophore development, we focused on the division of the protonemal apical stem cells that appear earlier than gametophores. Using time-lapse imaging of MTs and chromosomes, we observed severe MT phenotypes during the early stages of mitosis (Figure 4, Supplemental Video 3). During prophase, we detected a reduction in the number of perinuclear MTs (Figure 4E), which is also seen with a γ-tubulin RNAi (Nakaoka et al., 2012), and abnormal nuclear shape, which is unique to this mutant (elongated nucleus prior to NEBD, Figure 4C). After NEBD, 3 out of 52 cells in the RNAi lines failed to form bipolar spindles, followed by metaphase arrest and chromosome missegregation, which was never observed in control lines (Figure 4D). It is noteworthy that a similar phenotype was observed in 10% of the gametophore initial cells in the *TPX2-5 HM* line (Figure 3B, Supplemental Video 4). Other cells formed bipolar spindles; however, the number of MTs in the prometaphase spindle was greatly reduced (Figure 4F, blue). However, this was no longer the case at metaphase, where the number of MTs was similar to control spindles, indicating the recovery of MT numbers during prometaphase (Figure 4F, green). Phragmoplast formation and expansion were also similar to control cells. This is opposite to the findings in augmin-knockdown cells, in which the number of metaphase spindle MTs and phragmoplast MTs, but not prophase MTs, is reduced (Nakaoka et al., 2012). A plausible interpretation is that MTs were generated and reached control levels through γ-tubulin and augmin-dependent MT amplification during the prolonged prometaphase in the *TPX2* mutant (Petry et al., 2013). Thus, our results suggested that the role of TPX2 in MT amplification is dominant in early mitosis. As γ-tubulin activation motifs (Alfaro-Aco et al., 2017) are partially conserved in all moss TPX2 proteins (Figure 1B), we speculated that TPX2 is required for γ-tubulin-dependent MT nucleation in prophase and prometaphase, while augmin takes over from prometaphase. Other phenotypes observed upon TPX2 depletion included chromosome missegregation (29%) and spindle misposition/orientation (33%, Figure 4D, Supplemental Video 3). Overall, these phenotypes suggested the functional conservation of moss TPX2 with well-studied animal orthologues, namely assisting in MT formation through nucleation and/or stabilization.

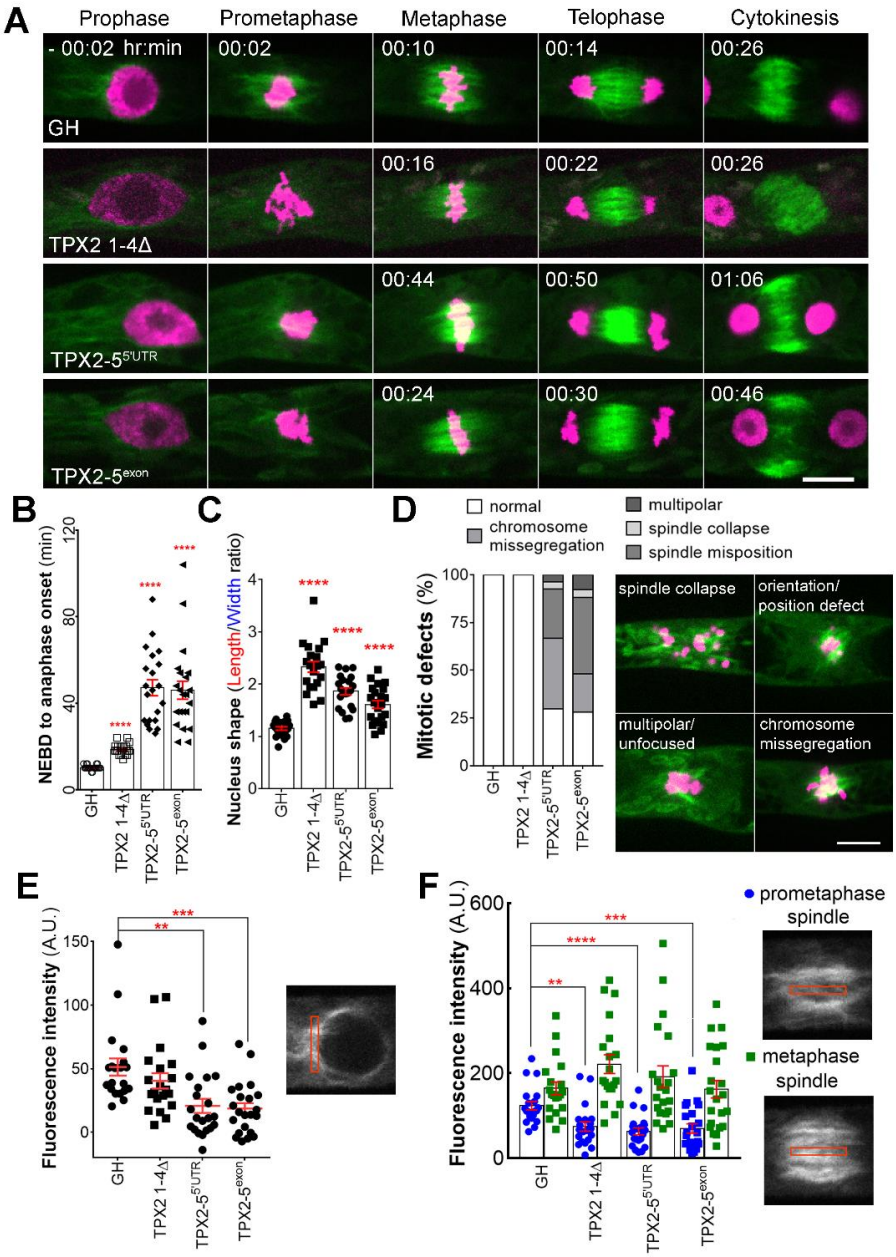

Figure 4. TPX2 contributed to microtubule amplification in early mitosis

(A) Representative images of the mitosis of protonemal apical cells in GH (control), *TPX2 1-4Δ*, *TPX2-5$^{5'UTR}$* RNAi, and *TPX2-5^{exon}* RNAi lines. Green, GFP-tubulin; Magenta, histoneH2B-mRFP. Bar, 10 µm. **(B)** Mitotic duration calculated from NEBD to anaphase onset (mean ± SEM; ****$p < 0.0001$, two-tailed Student's t-test). **(C)** Nucleus shape prior to NEBD, measured as a ratio of nucleus length to nucleus width (mean ± SEM; ****p < 0.0001, two-tailed Student's t-test). **(D)** Frequency and type of mitotic defects observed. Bar, 10 µm. **(E)** Fluorescence intensity of perinuclear MTs (mean ± SEM; **$p = 0.0011$, ***$p = 0.0002$; two-tailed Student's t-test). A.U. stands for Arbitrary Units. **(F)** Fluorescence intensity of MTs in the prometaphase spindle (4 min after NEBD) and metaphase spindle (2 min before anaphase onset), measured from a single focal plane, with the cytoplasmic background subtracted. A decrease in fluorescence intensity was detected in prometaphase, but not in metaphase spindles (mean ± SEM **$p = 0.0018$, ****$p \leq 0.0001$, ***$p = 0.0008$; two-tailed Student's t-test).

In plants, defective division sites have been mostly attributed to defects in PPB formation (Schaefer et al., 2017; Yoneda et al., 2005), phragmoplast guidance errors (CDZ deficiency) (Lipka et al., 2014; Müller, 2019), or abnormal positioning of the nucleus in prophase (Kimata et al., 2019; Yamada and Goshima, 2018). The current study identified an independent and hitherto-unappreciated cause of division site abnormality: spindle motility after NEBD. Furthermore, we identified a conserved protein, TPX2, as the critical player contributing to spindle positioning in plant cells. Interestingly, a recent study using neural stem cells of the embryonic developing mouse neocortex showed that TPX2 knockdown not only affects spindle MT generation but also spindle orientation, implicating a conserved TPX2-dependent mechanism of spindle positioning (Vargas-Hurtado et al., 2019). The spindle-specific positioning defect in meiosis II has also been observed in *jas* and *ps1* mutants of *Arabidopsis*, due to abnormal organelle distribution (Brownfield et al., 2015). However, meiosis II is a unique system where two spindles share a cytoplasm and may be partially fused in the absence of an organelle barrier. Therefore, there is unlikely to be a mechanistic analogy to the case of moss gametophores.

In addition to TPX2, this study uncovered the involvement of actin in spindle positioning. This was also an unexpected observation, as the function of actin in plant cell division has been mostly attributed to phragmoplast guidance during cytokinesis (Livanos and Müller, 2019; Rasmussen and Bellinger, 2018). However, actin is known to play an important role in spindle positioning in animal cells (Almonacid et al., 2014). Of particular interest are animal oocytes, as they also lack centrosomes. In mouse oocytes, spindle migration and symmetry breaking are driven by changes in the stability of the actin meshwork, the formation of which depends on actin nucleators, such as formin-2, and myosin II motor (Almonacid et al., 2014; Duan et al., 2020). Thus, an analogous mechanism may transmit force to transport spindles in moss. However, it should be noted that the role of actin emerged only in the background of a *TPX2* mutation. Thus, sufficient numbers of spindle MTs may predominate in the "tug-of-war" against actin-dependent forces in wild-type moss cells. A recent report suggests that spindle positioning can also take place in the absence of the PPB in seed plants, whose molecular mechanisms are unknown (Schaefer et al., 2017). TPX2 may be a promising candidate for investigations to elucidate the PPB-independent mechanism of cell division site positioning.

Materials and methods

P. patens culture and transformation

P. patens culture and transformation protocols are described in detail elsewhere (Yamada et al., 2016). In brief, BCDAT agar medium (BCDAT stands for stock solutions B, C, D and Ammonium Tartrate. Details can be found in (Yamada et al., 2016)) was used for regular culturing at 25°C under continuous light. Transformation was performed with a standard polyethylene glycol-mediated method using protoplasts. Transgenic lines were selected with corresponding antibiotics and confirmed by genotyping PCR or sequencing

in the case of CRISPR-generated lines. The GH line, expressing histone H2B-mRFP and GFP-α-tubulin, was used for transformation in the CRISPR and knockout experiments, while the mCherry-α-tubulin #52 line was used for Citrine and mNeonGreen endogenous tagging. The transgenic lines generated in this study are listed in Supplemental Table 1.

Molecular cloning

Plasmids for Citrine or mNeon-Green endogenous tagging were assembled using In-Fusion (Clontech, Mountain View, CA, USA), in which Citrine or mNeonGreen genes, a G418 resistance cassette (only C-terminal tagging), and homologous recombination regions (500-800 bp of the respective genes) were connected. A similar strategy was used for assembling the knockout plasmid for *TPX2-5*, wherein a hygromycin resistance cassette was flanked by the 5′- and 3′-UTR regions of the *TPX2-5* gene. A detailed protocol for endogenous gene tagging and knockouts in *P. patens* has been previously published (Yamada et al., 2016). CRISPR gRNAs, targeting one of the exons, were designed using the online tool, CRISPOR (http://crispor.tefor.net/), based on target gene specificity (off-target score) and predicted frameshift efficiency. Individual gRNAs were ligated into pCasGuide/pUC18 and pre-digested with BsaI. Next, gRNA sites, together with the *U6* promoter and gRNA scaffold regions, were amplified by PCR and assembled into a single multi-gRNA plasmid, also containing a hygromycin resistance cassette for transient plant selection. The detailed CRISPR protocol is described elsewhere (Leong et al., 2018). RNAi vectors were cloned using the Gateway system (Invitrogen, Carlsbad, CA, USA), with pGG624 as the destination vector. Two independent, non-overlapping RNAi constructs were prepared for each gene. The full list of plasmids and primers used in this study can be found in Supplemental Table 2.

Sample preparation for live-cell imaging

The sample preparation method for live-cell imaging is described in detail in a previous study (Yamada et al., 2016). In brief, a glass-bottom dish, coated with a thin layer of BCD agar medium (BCD stands for stock solutions B, C, D. Details can be found in (Yamada et al., 2016)), was inoculated with moss protonema and cultured under continuous light at 25°C prior to observation. For gametophore induction, 1 µM of the synthetic cytokinin, benzylaminopurine, diluted in 1 mL of distilled water, was added to the 6–7-day-old colony and incubated for 10 min. Next, the remaining liquid was aspirated with a pipette, the dish was sealed, and the sample was cultured as described above for 20–22 h prior to gametophore imaging. Latrunculin A and oryzalin were diluted in 1 mL of distilled water to final concentrations 5 µM and 200 nM, respectively. Prior to drug treatment, most of the agar pad from the glass-bottom dish was cut and removed to minimize the dilution. For cell membrane staining, FM4-64 was diluted in distilled water to a final concentration 10 µM and added to the live-imaging dish before acquisition, without cutting the agar. Imaging was performed immediately after drug application. For RNAi induction, 400 µL of 5 µM β-estradiol, diluted in distilled water, was added to the pre-cultured protonema,

4 d prior to observation. Note that, although β-estradiol was previously supplemented directly to the agar medium (Miki et al., 2016), we found that it almost entirely inhibited cell growth in *TPX2-5* RNAi lines; hence, the protocol was modified.

Microscopy and data analysis

Sample preparation is described above. Images were acquired using a Nikon Ti microscope (60 × 1.30-NA lens or 40 × 0.95-NA lens; Nikon, Tokyo, Japan) equipped with a CSU-X1 spinning-disk confocal unit (Yokogawa, Tokyo, Japan) and an electron-multiplying charge-coupled device camera (ImagEM; Hamamatsu, Hamamatsu, Japan). All imaging was performed at 22–24 °C in the dark, except for the first division of the gametophore initial, since gametophore development requires light (3-min light/2-min dark cycle). For single-leaf imaging, we dissected gametophores with syringe needles and scissors to isolate single leaves. Leaves were mounted in a drop of water between two coverslips and images were acquired with a Nikon Ti microscope (10 × 0.30-NA lens) in bright-field mode. The microscope was controlled using NIS-Elements software (Nikon) and image data were analyzed with ImageJ (National Institutes of Health, Bethesda, MD, USA). Prism software was used to plot the graphs and perform statistical analyses (GraphPad, San Diego, CA, USA). Gametophore and moss colony images were acquired after 4 weeks of culture using a stereoscopic microscope (Nikon SMZ800N) equipped with digital camera (ILCE-QX1α; Sony, Tokyo, Japan).

Sequence analysis

We used MAFFT ver. 7.043 (https://mafft.cbrc.jp/alignment/software/) to align the amino acid sequences of the selected full-length proteins and then manually revised them with MacClade ver. 4.08 OSX (www.macclade.org) to remove gaps. The Jones-Taylor-Thornton (JTT) model was used to construct maximum-likelihood trees in MEGA5 software (www.megasoftware.net). Statistical support for internal branches by bootstrap analyses was obtained using 1,000 replications. The gene sequence information discussed in this article is available under the following accession numbers in PHYTOZOME (www.phytozome.net): *At*TPX2 (AT1G03780.3); *Os*TPX2 (LOC_Os07g32390.1); *Pp*TPX2-1 (Pp3c17_11160V3.1); *Pp*TPX2-2 (Pp3c1_25950V3.1); *Pp*TPX2-3 (Pp3c24_8590V3.2); *Pp*TPX2-4 (Pp3c23_4540V3.1); *Pp*TPX2-5 (Pp3c5_10270V3.1); *Mp*TPX2-1 (Mapoly0016s0083.1); *Mp*TPX2-2 (Mapoly0105s0040.1) or in UNIPROT (www.uniprot.org): *Hs*TPX2 (Q9ULW0); *Gg*TPX2 (F1NW64); *Xl*TPX2 (Q6NUF4).

Acknowledgments

We would like to thank Momoko Nishina and Yuki Nakaoka for assistance with this project, Raymundo Alfaro-Aco for comments on the TPX2 functional motifs, Peishan Yi and Mariana Costa for helpful comments on the manuscript. This work was funded by JSPS KAKENHI (17H06471) and by JSPS and DFG under the Joint Research Projects-LEAD with UKRI (to G.G.). The authors declare no competing interests.

Author contributions

E.K. and G.G. designed the research project, E.K. and M.W.Y. performed experiments, E.K. analyzed the data, and E.K. and G.G. wrote the manuscript.

References

Alfaro-Aco R, Thawani A, Petry S. 2017. Structural analysis of the role of TPX2 in branching microtubule nucleation. *J Cell Biol* **177**:7–11. doi:10.1083/jcb.200611141

Almonacid M, Terret MÉ, Verlhac MH. 2014. Actin-based spindle positioning: New insights from female gametes. *J Cell Sci* **127**:477–483. doi:10.1242/jcs.142711

Ambrose JC, Cyr R. 2008. Mitotic spindle organization by the preprophase band. *Mol Plant* **1**:950–960. doi:10.1093/mp/ssn054

Arima K, Tamaoki D, Mineyuki Y, Yasuhara H, Nakai T, Shimmen T, Yoshihisa T, Sonobe S. 2018. Displacement of the mitotic apparatuses by centrifugation reveals cortical actin organization during cytokinesis in cultured tobacco BY-2 cells. *J Plant Res* **131**:803–815. doi:10.1007/s10265-018-1047-4

Bergstralh DT, Dawney NS, Johnston DS. 2017. Spindle orientation : a question of complex positioning. *Development* **5**:1137–1145. doi:10.1242/dev.140764

Boruc J, Deng X, Mylle E, Besbrugge N, Durme M Van, Demidov D, Tomaštíková ED, Tan T-RC, Vandorpe M, Eeckhout D, Beeckman T, Nowack M, Jaeger G De, Lin H, Liu B, Damme D Van. 2019. The TPX2-LIKE PROTEIN 3 is the primary activator of α Aurora kinases and is essential for embryogenesis. *Plant Physiol*. doi:10.1101/466276

Brownfield L, Yi J, Jiang H, Minina EA, Twell D, Köhler C. 2015. Organelles maintain spindle position in plant meiosis. *Nat Commun* **6**. doi:10.1038/ncomms7492

Buschmann H, Müller S. 2019. Update on plant cytokinesis: rule and divide. *Curr Opin Plant Biol* **52**:97–105. doi:10.1016/j.pbi.2019.07.003

Duan X, Li Y, Yi K, Guo F, Wang HY, Wu PH, Yang J, Mair DB, Morales EA, Kalab P, Wirtz D, Sun SX, Li R. 2020. Dynamic organelle distribution initiates actin-based spindle migration in mouse oocytes. *Nat Commun* **11**:277. doi:10.1038/s41467-019-14068-3

Kimata Y, Kato T, Higaki T, Kurihara D, Yamada T, Segami S, Morita MT, Maeshima M, Hasezawa S, Higashiyama T, Tasaka M, Ueda M. 2019. Polar vacuolar distribution is essential for accurate asymmetric division of Arabidopsis zygotes. *Proc Natl Acad Sci U S A* **116**:2338–2343. doi:10.1073/pnas.1814160116

Kiyomitsu T. 2019. The cortical force-generating machinery: how cortical spindle-pulling forces are generated. *Curr Opin Cell Biol* **60**:1–8. doi:10.1016/j.ceb.2019.03.001

411 Kosetsu K, Murata T, Yamada M, Nishina M, Boruc J, Hasebe M, Van Damme D,
412 Goshima G. 2017. Cytoplasmic MTOCs control spindle orientation for asymmetric
413 cell division in plants. *Proc Natl Acad Sci* **114**:E8847–E8854.
414 doi:10.1073/pnas.1713925114

415 Leong SY, Yamada M, Yanagisawa N, Goshima G. 2018. SPIRAL2 Stabilises
416 Endoplasmic Microtubule Minus Ends in the Moss *Physcomitrella patens*. *Cell*
417 *Struct Funct* **43**:53–60. doi:10.1247/csf.18001

418 Lipka E, Gadeyne A, Stöckle D, Zimmermann S, De Jaeger G, Ehrhardt DW, Kirik V,
419 Van Damme D, Müller S. 2014. The phragmoplast-orienting kinesin-12 class
420 proteins translate the positional information of the preprophase band to establish
421 the cortical division zone in Arabidopsis thaliana. *Plant Cell* **26**:2617–2632.
422 doi:10.1105/tpc.114.124933

423 Livanos P, Müller S. 2019. Division Plane Establishment and Cytokinesis. *Annu Rev*
424 *Plant Biol* **70**:239–267. doi:10.1146/annurev-arplant-050718-100444

425 Martinez P, Luo A, Sylvester A, Rasmussen CG. 2017. Proper division plane
426 orientation and mitotic progression together allow normal growth of maize. *Proc*
427 *Natl Acad Sci U S A* **114**:2759–2764. doi:10.1073/pnas.1619252114

428 Miki T, Nakaoka Y, Goshima G. 2016. Live Cell Microscopy-Based RNAi Screening in
429 the Moss Physcomitrella patens. *Methods Mol Biol* **1470**:225–246.
430 doi:10.1007/978-1-4939-6337-9_18

431 Moody LA, Kelly S, Rabbinowitsch E, Langdale JA. 2018. Genetic Regulation of the
432 2D to 3D Growth Transition in the Moss Physcomitrella patens. *Curr Biol* **28**:473-
433 478.e5. doi:10.1016/j.cub.2017.12.052

434 Müller S. 2019. Plant cell division — defining and finding the sweet spot for cell plate
435 insertion. *Curr Opin Cell Biol* **60**:9–18. doi:10.1016/j.ceb.2019.03.006

436 Nakaoka Y, Miki T, Fujioka R, Uehara R, Tomioka A, Obuse C, Kubo M, Hiwatashi Y,
437 Goshima G. 2012. An Inducible RNA Interference System in Physcomitrella
438 patens Reveals a Dominant Role of Augmin in Phragmoplast Microtubule
439 Generation. *Plant Cell* **24**:1478–1493. doi:10.1105/tpc.112.098509

440 Ôta T. 1961. The Role of Cytoplasm in Cytokinesis of Plant Cells. *Cytologia* **26**:428–
441 447. doi:10.1508/cytologia.26.428

442 Petry S. 2016. Mechanisms of Mitotic Spindle Assembly. *Annu Rev Biochem* **85**:659–
443 683. doi:10.1146/annurev-biochem-060815-014528

444 Petry S, Groen AC, Ishihara K, Mitchison TJ, Vale RD. 2013. Branching microtubule
445 nucleation in xenopus egg extracts mediated by augmin and TPX2. *Cell* **152**:768–
446 777. doi:10.1016/j.cell.2012.12.044

447 Rasmussen CG, Bellinger M. 2018. An overview of plant division-plane orientation.
448 *New Phytol* **219**:505–512. doi:10.1111/nph.15183

449 Schaefer E, Belcram K, Uyttewaal M, Duroc Y, Goussot M, Legland D, Laruelle E, De
450 Tauzia-Moreau ML, Pastuglia M, Bouchez D. 2017. The preprophase band of

microtubules controls the robustness of division orientation in plants. *Science* **356**:186–189. doi:10.1126/science.aal3016

Smertenko A, Assaad F, Baluška F, Bezanilla M, Buschmann H, Drakakaki G, Hauser MT, Janson M, Mineyuki Y, Moore I, Müller S, Murata T, Otegui MS, Panteris E, Rasmussen C, Schmit AC, Šamaj J, Samuels L, Staehelin LA, Van Damme D, Wasteneys G, Žárský V. 2017. Plant Cytokinesis: Terminology for Structures and Processes. *Trends Cell Biol* **27**:885–894. doi:10.1016/j.tcb.2017.08.008

Tomaštíková E, Demidov D, Jeřábková H, Binarová P, Houben A, Doležel J, Petrovská B. 2015. TPX2 Protein of Arabidopsis Activates Aurora Kinase 1, But Not Aurora Kinase 3 In Vitro. *Plant Mol Biol Report* **33**:1988–1995. doi:10.1007/s11105-015-0890-x

Vargas-Hurtado D, Brault JB, Piolot T, Leconte L, Da Silva N, Pennetier C, Baffet A, Marthiens V, Basto R. 2019. Differences in Mitotic Spindle Architecture in Mammalian Neural Stem Cells Influence Mitotic Accuracy during Brain Development. *Curr Biol* **29**:2993-3005.e9. doi:10.1016/j.cub.2019.07.061

Verma DPS. 2001. Cytokinesis and building the cell wall in plants. *Annu rev plant Physiol* **52**:751–784.

Vos JW, Pieuchot L, Evrard J-L, Janski N, Bergdoll M, De Ronde D, Pérez LH, Sardon T, Vernos I, Schmit A-C. 2008. The Plant TPX2 Protein Regulates Prospindle Assembly before Nuclear Envelope Breakdown. *Plant Cell* **20**:2783–2797. doi:10.1105/tpc.107.056796

Yamada M, Goshima G. 2018. The KCH kinesin drives nuclear transport and cytoskeletal coalescence to promote tip cell growth in Physcomitrella patens. *Plant Cell* **30**:1496–1510. doi:10.1105/tpc.18.00038

Yamada M, Miki T, Goshima G. 2016. Imaging Mitosis in the Moss Physcomitrella patens. *Methods Mol Biol* **1413**:293–326. doi:10.1007/978-3-319-02904-7

Yi P, Goshima G. 2019. Transient cotransformation of CRISPR /Cas9 and oligonucleotide templates enables efficient editing of target loci in Physcomitrella patens . *Plant Biotechnol J* 1–3. doi:10.1111/pbi.13238

Yoneda A, Akatsuka M, Hoshino H, Kumagai F, Hasezawa S. 2005. Decision of spindle poles and division plane by double preprophase bands in a BY-2 cell line expressing GFP-tubulin. *Plant Cell Physiol* **46**:531–538. doi:10.1093/pcp/pci055

Supplemental Data

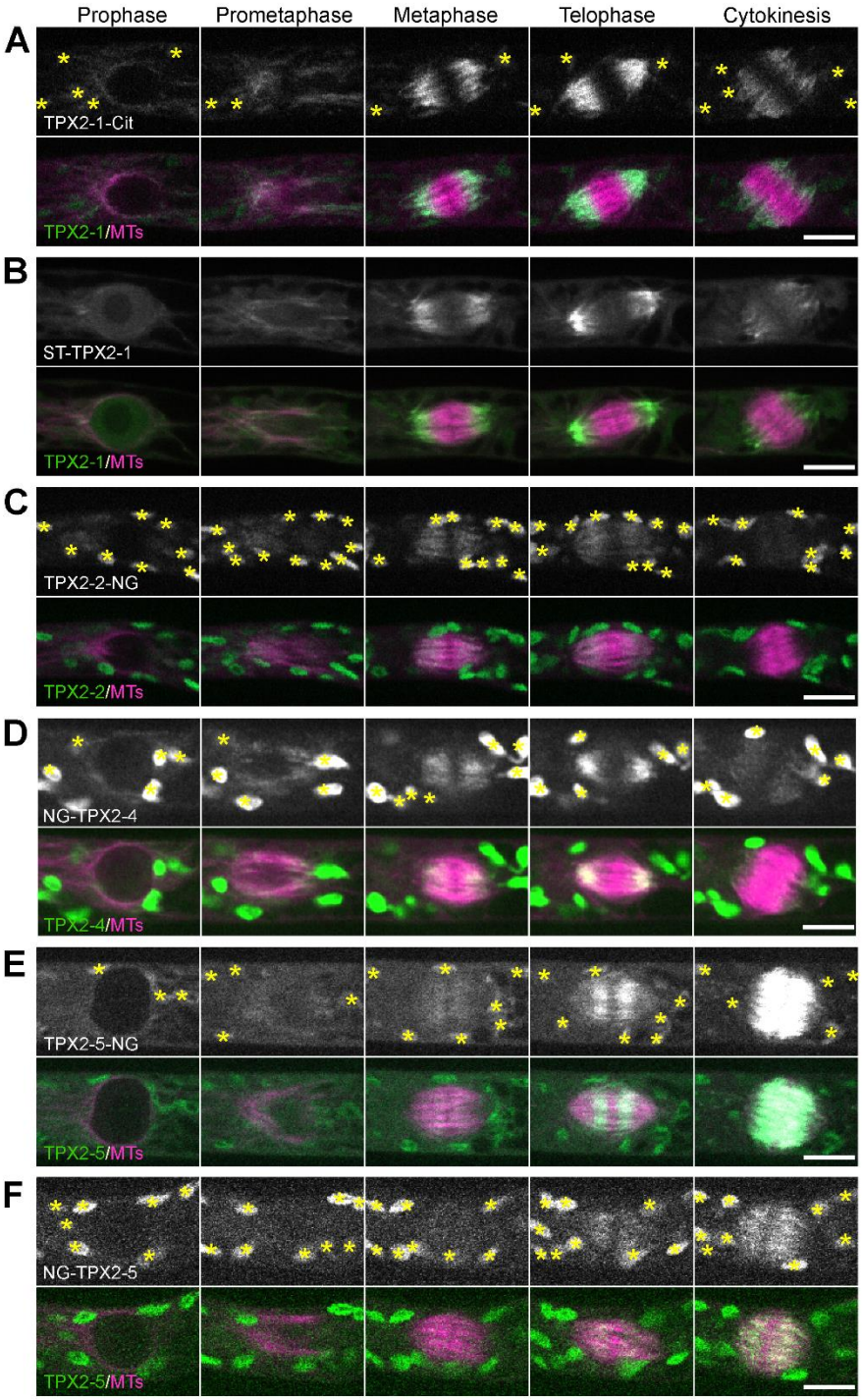

Supplemental Figure 1. Localization of TPX2 proteins during mitosis

Live-cell imaging was performed in caulonemal apical cells of *P. patens*, expressing mCherry-tubulin and one of the following TPX2 proteins endogenously tagged with a fluorophore: (A) TPX2-1-Citrine; (B) SunTag-TPX2-1; (C) TPX2-2-mNeonGreen; (D) mNeonGreen-TPX2-4; (E) TPX2-5-mNeonGreen; (F) mNeonGreen-TPX2-5. The SunTag-TPX2-1 line also expressed scFv-GCN-sfGFP under a β-estradiol-inducible promoter. Asterisks indicate autofluorescent chloroplasts. Bars, 10 µm.

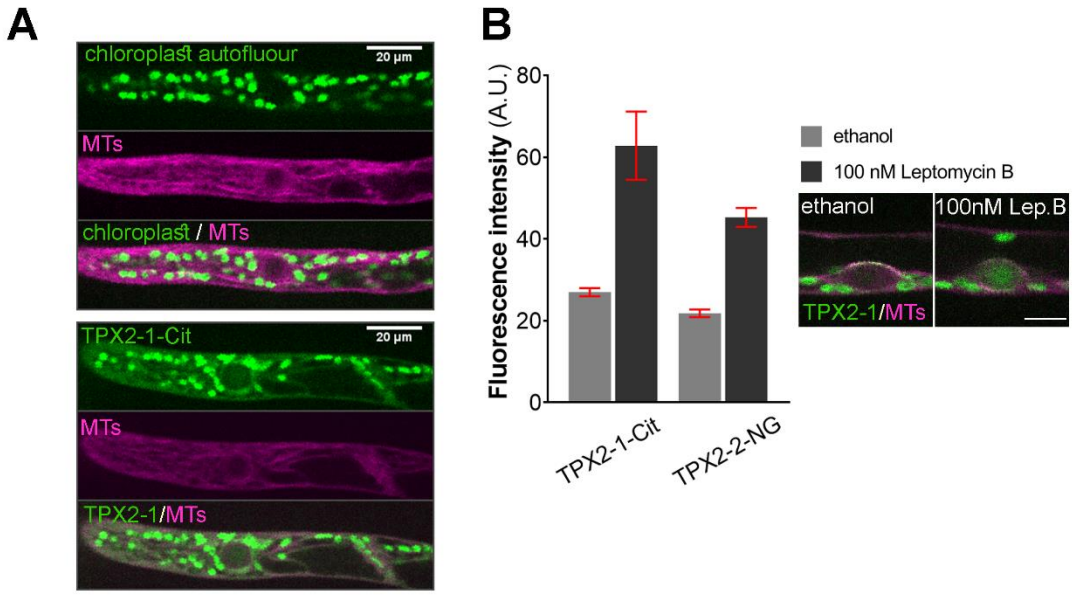

Supplemental Figure 2. Interphase localization of TPX2

(A) Live-cell imaging was performed in caulonemal apical cells of *P. patens*, expressing only mCherry-tubulin (upper panels) or mCherry-tubulin and TPX2-1-Citrine (bottom panels). Cytoplasmic signals increased in the TPX2-1-Citrine line. Bars, 20 µm. **(B)** Fluorescence intensity in the nucleus before and after inhibiting nuclear export with 100 nM Leptomycin B (mean ± SEM) after subtracting the cytoplasmic background. Increase in nuclear signals after nuclear export inhibition suggests that TPX2-1-Cit and TPX2-2-NG are actively shuttled between the nucleus and cytoplasm.

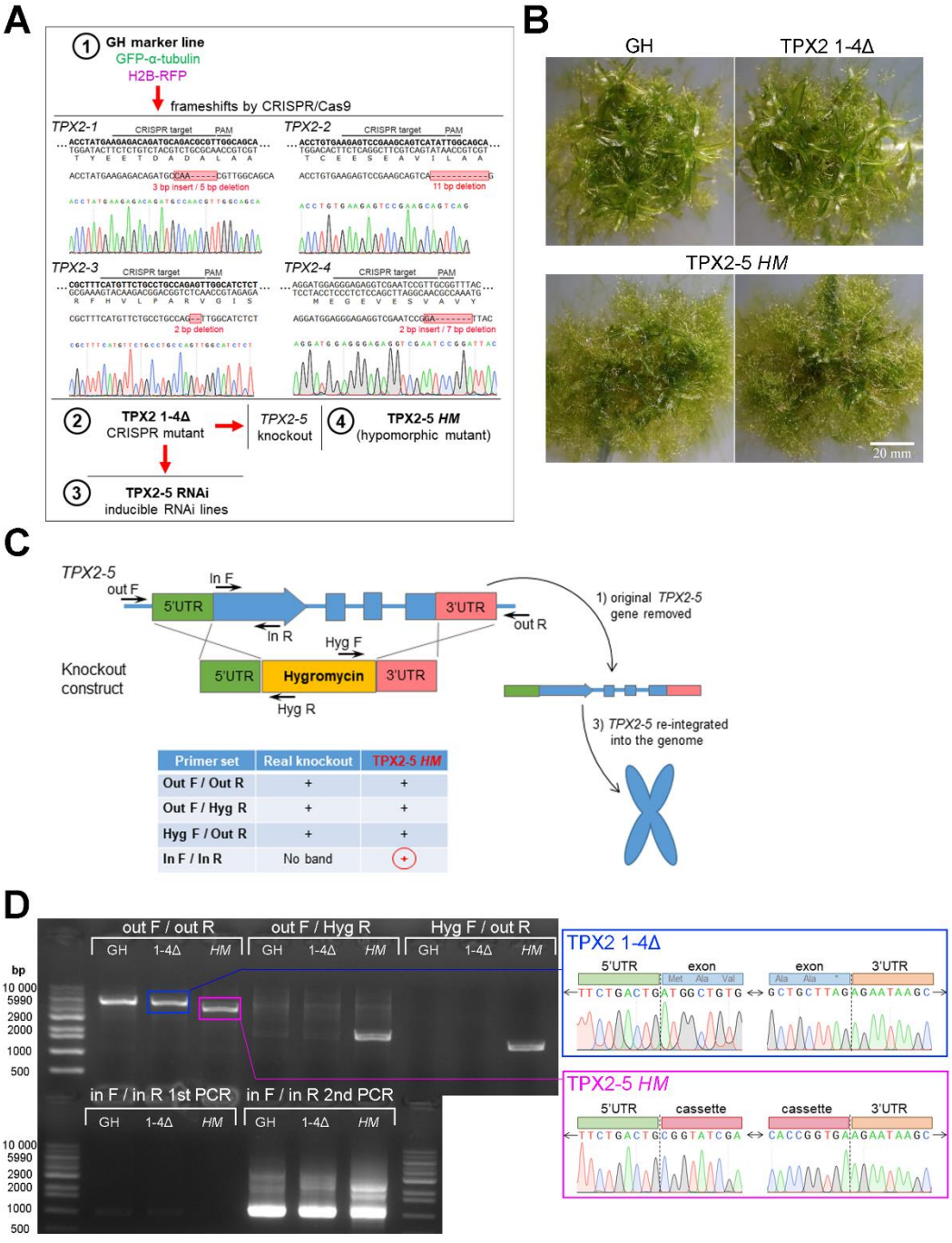

Supplemental Figure 3. Isolation of hypomorphic *TPX2* mutants

(A) Schematic explanation of *P. patens* lines created and used in this study and representative sequencing data of frameshift mutations in the *TPX2 1-4Δ* line. **(B)** Representative colonies of GH (control), *TPX2 1-4Δ* (CRISPR frameshift mutant), and TPX2-5 *HM* (hypomorphic mutant). The *TPX2 1-4Δ* line is indistinguishable from wild-type moss, while TPX2-5 *HM* has dwarf gametophores. Bar, 20 mm. **(C)** Schematic explanation of *TPX2-5* knockout experiments, *TPX2-5 HM* line selection, and genotyping PCR. **(D)** Results of genotyping PCR and sequencing of the *TPX2-5* locus. For unknown reasons, first round of F/in R PCR yielded barely visible bands and therefore, we performed a second round of PCR using diluted product of the first PCR as the template.

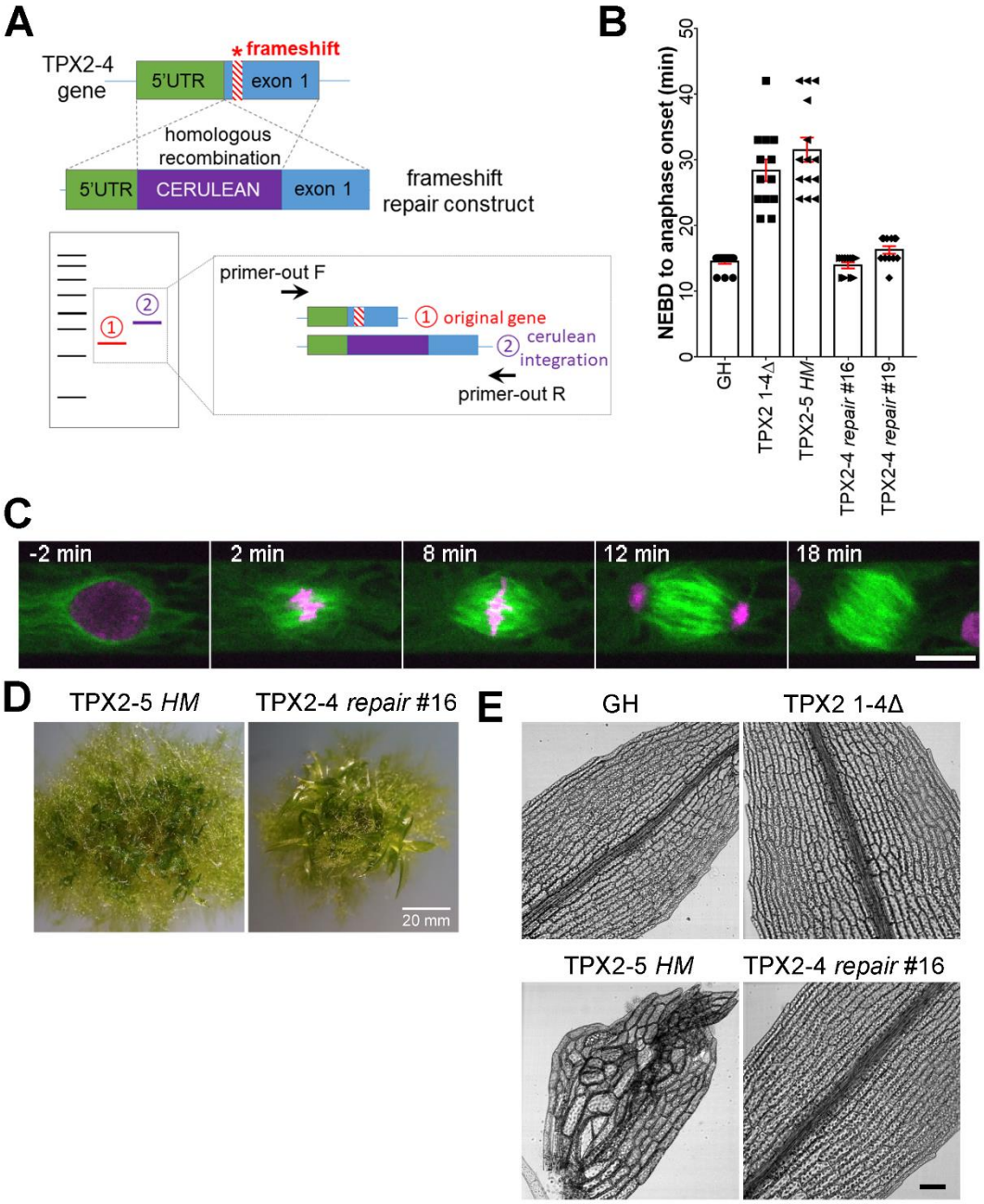

Supplemental Figure 4. Rescue of the *TPX2-5 HM* phenotypes by frameshift repair of the *TPX2-4* gene

(A) Schematic illustration of the frameshift repair experiment. In brief, the N-terminus-coding region of the *TPX2-4* gene was tagged with Cerulean flanked with ~500 bp of the 5′-UTR and exon region (without the frameshift mutation) by homologous recombination. Construct integration was verified by PCR. **(B)** Mitotic duration of protonemal cells calculated from NEBD to anaphase onset in GH, *TPX2 1-4Δ*, *TPX2-5 HM*, and two independent *TPX2-4* repair lines (mean ± SEM). **(C)** Mitotic progression in the *TPX2-4* repair #16 line. Note that perinuclear MTs and prometaphase spindle formation were restored. Bar, 10 µm. **(D)** Representative images of the *TPX2-5 HM* colony with dwarf gametophores and a *TPX2-4* repair #16 colony with normal gametophores. **(E)** Representative images of gametophore leaf cells in GH, *TPX2 1-4Δ*, *TPX2-5 HM*, and *TPX2-4* repair #16 lines. Bar, 100 µm.

Supplemental Video 1. Localization of TPX2 proteins during mitosis
Live-cell imaging was performed in *P. patens* apical caulonemal cells expressing mCherry-tubulin (magenta) and one of the following tagged proteins (green): TPX2-1-Citrine, TPX2-2-mNeonGreen, mNeonGreen-TPX2-4, or TPX2-5-mNeonGreen. Images were acquired every 30 s at a single focal plane. Bar, 10 µm.

Supplemental Video 2. Spindle motility underlies the erroneous phragmoplast positioning in *TPX2-5 HM* gametophore initial cells
Live-cell imaging was performed in *P. patens* gametophore initial cells expressing mCherry-tubulin and Histone H2B-mCherry (chromosomes and MTs are labeled with the same color). Images were acquired as a z-stack (20 µm, 2.5 µm step) every 5 min and the best focal plane is presented. Bar, 10 µm.

Supplemental Video 3. Mitotic defects in the *TPX2-5* RNAi line
Representative images of mitotic defects in the *TPX2-5* RNAi lines. Live-cell imaging was performed in *P. patens* protonemal apical cells expressing GFP-tubulin (green) and histone H2B-mCherry (magenta). Images were acquired at a single focal plane every 2 min. Bar, 10 µm.

Supplemental Video 4. Spindle-collapse phenotype in the gametophore initial of *TPX2-5 HM* mutants
Representative video of spindle collapse followed by chromosome missegregation, observed in approximately 10% of *TPX2-5 HM* gametophore initial cells. Images were acquired as a z-stack (20 µm, 2.5 µm step) every 5 min and the best focal plane is presented. Bar, 10 µm.